Results in Physics 51 (2023) 106752

Contents lists available at ScienceDirect

Results in Physics

journal homepage: www.elsevier.com/locate/rinp

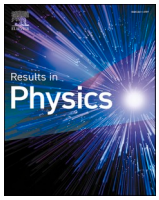

Radiation characterizations of two isotopic neutron sources merging in one irradiator for experimental applications in the laboratory

Mohammed M. Damoom [a,b,*], Abdulsalam M. Alhawsawi [a,b], Essam Banoqitah [a,b], Mohammed Siddig H. Mohammed [a], Eslam Taha [a,b], Yahya Z. Hazzaa [a], Rayan B. Fawrah [a], M.M.T. Qutub [a,b], Abdu Saeed [c,d,*]

[a] Nuclear Engineering Department, King Abdulaziz University, Jeddah 21589, Saudi Arabia
[b] Center for Training & Radiation Protection, King Abdulaziz University, Jeddah 21589, Saudi Arabia
[c] Department of Physics, Faculty of Science, King Abdulaziz University, Jeddah 21589, Saudi Arabia
[d] Department of Physics, Thamar University, Thamar 87246, Yemen

ARTICLE INFO

Keywords:
^{241}Am-^{9}Be source
Monte Carlo calculation
Neutron flux
Neutron activation

ABSTRACT

Neutron sources are utilized for different aims, such as studying the material's internal structure, investigating the materials' crystal structures, and neutron therapy. Using more than one isotopic neutron source in some aims could be beneficial. Herein, a neutron irradiator consisting of two ^{241}Am-^{9}Be neutron sources has been designed. Radiation characterizations, including the neutron fluence and dose rate, were investigated. The Monte Carlo simulation code Monte Carlo N-particle transport code version 5 (MCNP5) was used to conduct all the required investigations to achieve an optimal design. Two factors were considered; the first was the dose rate due to both neutron and gamma radiations to meet radiation protection requirements; MCNP5 was used to determine the adequate thickness of the shielding material. The second parameter is the neutron fluence. Two irradiation sites have been proposed, one for fast neutron irradiation and the other for thermal neutron irradiation. By utilizing MCNP5, we have determined the radiation characterization at the two sites to be used as the irradiation sites. After the optimal design had been produced, the thermal and the epithermal neutron fluences inside the two irradiation sites were determined experimentally. The experimental results showed a perfect agreement with the simulation ones. The neutron irradiator designed from merged two isotopic neutron sources could be a benefit in the neutron radiation applications in the labs.

Introduction

Neutrons have played an essential role in science and engineering since they were discovered in 1932. Neutron sources can be reactors, 14-MeV neutron generators [1], and isotopic neutron sources [2], which can be alpha or gamma–neutron sources; ^{241}Am-^{9}Be and ^{124}Sb-^{9}Be are examples of them, respectively [2]. In isotopic neutron sources, radioisotopes can be used to induce neutron emission from a target low-Z nuclide material, in which their neutrons' binding energies are low [2]. Also, isotopic neutron sources can be spontaneous fission sources such as ^{252}Cf [3]. Also, neutrons can be produced via a process called spallation [4,5].

The importance of neutron sources comes being using the neutron for different purposes [6–9]. Where neutron diffraction is used to study other materials' magnetic [8] and crystal structures [9]. Additionally, neutron imaging is used as a non-destructive method to study rocks [10]. Neutron radiation is used for scientific research aims, such as irradiating samples [11–14] and animals [15–19] and exploring the crystal structure of prepared samples [20]. Furthermore, neutrons are used in medical applications such as boron neutron capture therapy. Additionally, neutron sources are utilized in neutron activation analysis (NAA), which mainly depends on neutrons to combine with a stable nucleus (in the ground state), which becomes excited. This nucleus is then de-excited by emitting gamma rays, which act as fingerprints for the activated nucleus [21]. NAA is used in various applications, such as archaeology and environmental samples [22].

Based on the aforementioned different neutrons' uses, neutron sources are urgently needed. However, the reactors for those mentioned

* Corresponding authors at: Nuclear Engineering Department, King Abdulaziz University, Jeddah 21589, Saudi Arabia (M.M. Damoom); Department of Physics, Faculty of Science, King Abdulaziz University, Jeddah 21589, Saudi Arabia (A. Saeed).
E-mail addresses: mdamoom@kau.edu.sa (M.M. Damoom), Abdusaeed79@tu.edu.ye, Abdusaeed79@hotmail.com (A. Saeed).

https://doi.org/10.1016/j.rinp.2023.106752
Received 23 May 2023; Received in revised form 10 July 2023; Accepted 11 July 2023
Available online 17 July 2023

Table 1
Materials, their densities, and the corresponding cross-section libraries for each element.

Material		Weight fraction	Density (g. cm^{-3})	Cross-section library
Name	Isotope			
HDPE	^{1}H S(α, β)	0.14	0.93	poly.60 t, 1001.42c
	^{12}C	0.86		6012.42c
Lead	Pb	1.00	11.30	82000.42c
Iron	^{56}Fe	1.00	8.00	26056.42c
^{241}Am-^{9}Be	^{241}Am	0.07	1.5	95241.60c
	^{9}Be	0.93		4009.60c

applications are unavailable in most countries, and access to such facilities is not easy in other countries. On the other hand, building 14-MeV neutron generators as the neutron source everywhere in any country is very costly. Therefore, isotopic neutron sources are a practical and reasonable solution to get neutrons in conventional labs. Unfortunately, these isotopic neutron sources have low neutron yields; their flux is very low compared with research reactors [23,24]. Therefore, merging more than isotopic neutron sources to build a neutron irradiator, particularly in the research labs, could be a feasible idea.

In this study, we utilized two isotopic neutron sources to build a neutron irradiator for experiments involving neutron radiation; this built neutron irradiator can be used for both irradiation and activation. We used two ^{241}Am-^{9}Be sources to achieve this goal; a chamber (irradiator) was designed to host them. This irradiator fulfills two requirements: first, it provides an adequate shield against neutron and gamma radiations due to both sources; second, it must facilitate the neutron irradiation process. We used the Monte Carlo N-particle transport code, version 5 (MCNP5), to achieve these two requirements in the neutron irradiator with the optimal design. After designing the neutron irradiator, radiation characterizations such as neutron fluences and dose rates were measured experimentally and compared with the simulated ones. The details of the radiation characterizations of the built irradiator were included in the following sections.

Methodology

^{241}Am-^{9}Be neutron sources

The ^{241}Am-^{9}Be source is an (α, n) neutron source type with a half-life of 432 years. It is widely used in many fields, such as neutron activation analysis, calibration, scientific research, and industrial applications [25–28]. The source strength of 1 Ci of ^{241}Am-^{9}Be is 2.2×10^{6} neutrons/second ($n.s^{-1}$) [23]. ^{241}Am atoms emit alpha particles, which combine with ^{9}Be atoms forming a compound nucleus of ^{13}C, which decays into an exited ^{12}C nucleus and a neutron according to the following nuclear reaction [29]:

$$\alpha+\frac{9}{4}\mathrm{Be}\rightarrow\frac{13}{6}\mathrm{C}^{*}\rightarrow\frac{12}{6}\mathrm{C}+\mathrm{n} \quad (1)$$

The ^{241}Am-^{9}Be source emits neutrons with a broad spectrum of energies up to 10 MeV with an average energy of 4.5 MeV [30,31]. We used two sources of ^{241}Am-^{9}Be to be merged as one irradiator; they were with two radiation activities of 5 and 3 Ci; the source with the large value activity was named source 1, and the small was named source 2.

The two ^{241}Am-^{9}Be neutron sources were modeled as cylinders of 26 and 18 mm in diameter and 54 and 46 mm in height. They were capsulated with 4 mm of stainless steel. The ISO-8529–1 report was utilized for the emerging neutron spectrum of the ^{241}Am-^{9}Be neutron source. Table 1 represents the materials, their densities, and the cross-section libraries that were used to model the irradiator and the Am-Be sources.

Monte Carlo method simulation

Different Monte Carlo Method codes, such as MCNP, Geant4, and Fluka, are used to simulate radiation transport through materials. We used the MCNP5 code, which has powerful capabilities for simulating radiation transport within materials. Some powerful MCNP tools were used in this work, such as mesh tally, F4 tally type, and neutron capture calculation within the foil gold, ^{97}Au(n,γ)^{198}, to compare the simulation results with the experimental results.

The tally type (mesh) was used to calculate the average fluence and other parameters over mesh cells in units of particles/cm^{2}. This tally type facilitates generating an image of flux, multiplying the fluence by the source strength 1.76×10^{7}n.s^{-1} or other radiation parameters. According to the irradiation selected sites, the mesh was used to map the neutron flux inside the irradiator.

The tally type (F4) is used to calculate the average particle (neutron, photon… etc.) fluence in a cell. Later, many parameters can be deduced from this fluence, such as flux and dose rate. This tally type (F4) was used to calculate the fluence, spectrum, and dose rate of neutrons and gamma rays in the selected irradiation sites.

For calculating the effective dose rate, the flux-to-dose conversion factors published in ICRP 74 report were adopted. These conversion factors are multiplied by the resultant fluences and the source strength to generate the effective dose rate.

Radiation protection precautions

The final design of the irradiator must keep the radiation dose rate at 1 m away from the outer surface within the permissible limits that recommended by the IAEA for occupational exposure due to all radiation types. IAEA recommendation is not to exceed 20 mSv per year as occupational exposure. Accordingly, the dose rate limit must not exceed 10 μSv/hr in case of 2000 working hours a year. Therefore, the adequate dimensions of the material used to build up the irradiator must be figured out first. The ^{241}Am-^{9}Be source emits neutrons and gamma rays beside alpha particles [23,29]. All alpha particles are absorbed inside the source capsule. Consideration should be paid to the neutron and gamma rays because of their high penetration even throughout the solid matter.

Hydrogenous materials are commonly used to shield against fast neutrons. High-density polyethylene (HDPE), C_2H_4, is a famous hydrogenous material utilized in neutron shielding [32]; it is a good material for neutron shielding with a lighter weight and low cost. The sufficient thickness of the HDPE was calculated by MCNP5 code; the estimated thickness was enough to reduce the neutron dose rate outside the irradiator to or less than the permissible limits.

Regarding the gamma rays emerging from the sources, the 4.4 MeV gamma ray is the most hazardous one that must be considered. This gamma-ray yield is about 0.6% of the neutrons yield [24,29,33]. We used the lead (Pb) as a gamma-ray shield. Also, the appropriate thickness of Pb was worked out throughout the MCNP5 simulation.

To reach the optimal dimensions, the following procedures were conducted. The proposed initial thickness of HDPE was 25 cm which did not fulfill the requirements, so this process was repeated several times until that requirement was met. Also, an initial thickness of lead was suggested to be 1 cm; each time, the effective dose rate was checked; in case the thickness was not enough, then the thickness was increased till the permissible limit was reached.

Neutron fluence mapping

After the optimal dimensions of the irradiator had been determined, the next step was to find the best positions for the irradiation sites. This work proposed two irradiation sites: one for fast neutron irradiation and the other for thermal irradiation.

The mesh tally is one of the powerful tools in MCNP5; this tally was

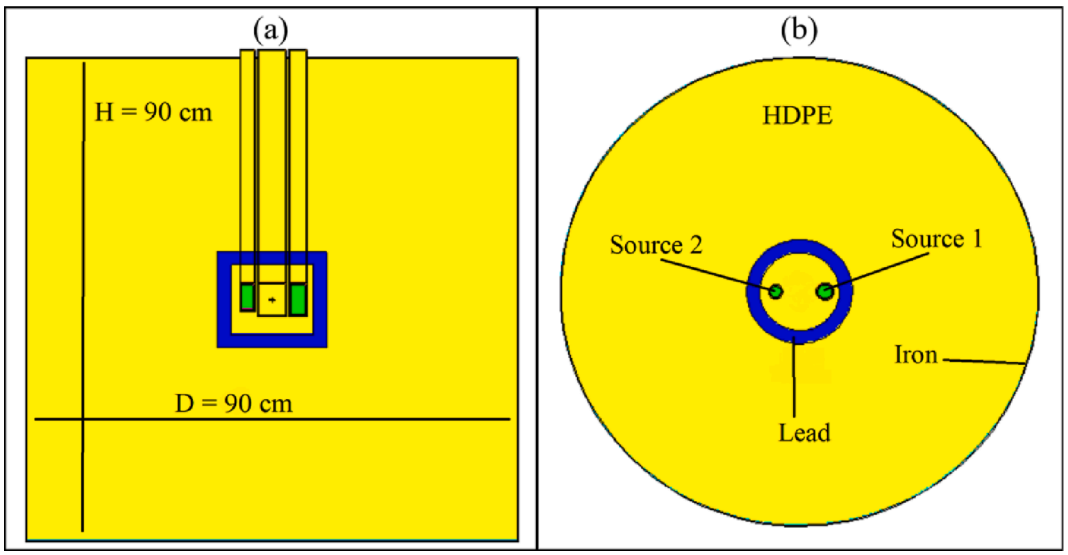

Fig. 1. (a) A cross-section view, (b) a top view of the final optimal design of the irradiator.

used to generate a map of fluence distribution for the three components of the neutron spectrum: fast, epithermal, and thermal fluences. The mesh tally was set to cover an area of 20 cm by 20 cm around the center of the irradiator; the resolution of this mesh tally was adjusted to 100 by 100. After the two irradiation sites had been determined, the radiation features, i.e., the neutron spectrum and fluence, the gamma-ray spectrum, and the radiation exposure due to neutron and gamma rays, were characterized.

Radiation spectra and dose rate in irradiation sites

The F4 tally type is one of the tools in MCNP5; it was used to calculate the neutron spectrum at both irradiation sites. The simulation resultant for the neutron spectra revealed that the spectrum could be divided into three regions: The first one is thermal flux, whose energies are equal to or less than the cadmium cut-off energy of 0.55 eV; the second is epithermal neutron flux, which is between the range of 0.55 eV and 0.1 MeV; the third is the fast neutron flux that has energy exceeding 0.1 MeV.

Gamma-ray spectra in the irradiation sites were also calculated using the F4 tally type. In this work, there are two components of gamma rays. Firstly, gamma rays come directly from the ^{241}Am-^{9}Be source, particularly the 4.44 MeV that comes from the first excited state of ^{12}C. Secondly, gamma rays emerge due to the interaction between neutrons and irradiator materials (prompt gamma). An example is 2.22 MeV, which is attributable to thermal neutron capture by hydrogen.

NAa

Although NAA has become an indispensable analysis tool in many fields because of its sensitivity and accuracy in determining tracer chemical elements in samples, it is an essential application for estimating the thermal and epithermal flux in irradiation facilities [34–36]. In NAA, foils are utilized for radiation characterizations, such as flux determination, spectral measurement, and dosimetry. For instance, elements such as gold, indium, aluminum, and scandium are used as neutron activation foils [36–38]. Bare and cadmium-covered gold foils in this work were utilized to estimate the thermal and epithermal flux. The bare and cadmium-covered gold foils (10 mm in diameter and 0.1 mm thick) were inserted into the neutron beam path; then, the flux was determined by measuring the delayed emitted gamma rays (411 keV) due to the reaction ^{197}Au(n,γ)^{198}Au. Where hundreds of gamma rays emerge due to the ^{197}Au(n,γ)^{198}Au reaction, these gamma rays are prompt, but three are delayed with a half-life of 2.7 days; these three are 411.8, 675.884, and 1,087.684 keV with cross-sections of 94.3, 0.793, and 0.157b, respectively [39].

The thermal (σ_{Th}) and epithermal (σ_{Epi}) capture of ^{197}Au(n, γ)^{198}Au reaction average microscopic cross-sections were calculated in both irradiation sites using the below formula:

$$\overline{\sigma} = \frac{\sum_{i=1}^{n}\sigma(E_i)\varphi(E_i)}{\sum_{i=1}^{n}\varphi(E_i)} \tag{2}$$

where $\sigma(E_i)$ is the microscopic cross-section of radiative capture of the neutron with energy group i by the nucleus ^{197}Au; $\varphi(E_i)$ is the neutron flux spectrum with energy group i obtained in the irradiation site. Both the microscopic cross-section of radiative capture and the neutron spectrum in the irradiation sites were divided into several same groups to facilitate the use of Eq. (2), By setting $E_{min} = 0$ and $E_{max} = 0.55$ eV for the thermal part and $E_{min} = 0.55$ eV and $E_{max} = 0.1$ MeV for the epithermal part of the neutron spectrum. It was found that the $\sigma_{th} = 83.7$ and $\sigma_{Epi} = 25.3$ barns.

Estimation of the neutron flux

After the activities of both the bare and the covered gold foils were obtained in the previous step, both flux components, thermal and epithermal, were estimated using the following equations [40]:

$$\varphi_{Th} = \frac{A_{ba}F_{cd}e^{\lambda t_2}}{\overline{\sigma}_{Th}NG_{Th}(1-e^{-\lambda t_1})} \tag{3}$$

where $F_{cd} = \frac{R_{cd}-1}{R_{cd}}$; $R_{cd} = \frac{A_{bar}}{A_{cd}}$

$$\varphi_{Epi} = \frac{A_{cd}e^{\lambda t_2}}{\overline{\sigma}_{Epi}NG_{Epi}(1-e^{-\lambda t_1})} \tag{4}$$

Where A_{bc} and A_{cd} are the bare and covered gold foil activity, respectively. $\overline{\sigma}_{Th}$ and $\overline{\sigma}_{Epi}$ are the thermal and epithermal neutrons averages capture cross-sections, respectively. N is the total atoms of ^{197}Au in the gold foil; λ is the decay constant of ^{198}Au; t_1 and t_2 represent the irradiation time and time from withdrawing the foil from the irradiation facility to putting it on the high purity germanium (HPGe) detector. G_{th} and G_{th} are the self-shielding of thermal and epithermal neutrons, respectively. They were estimated according to the following equations [41]:

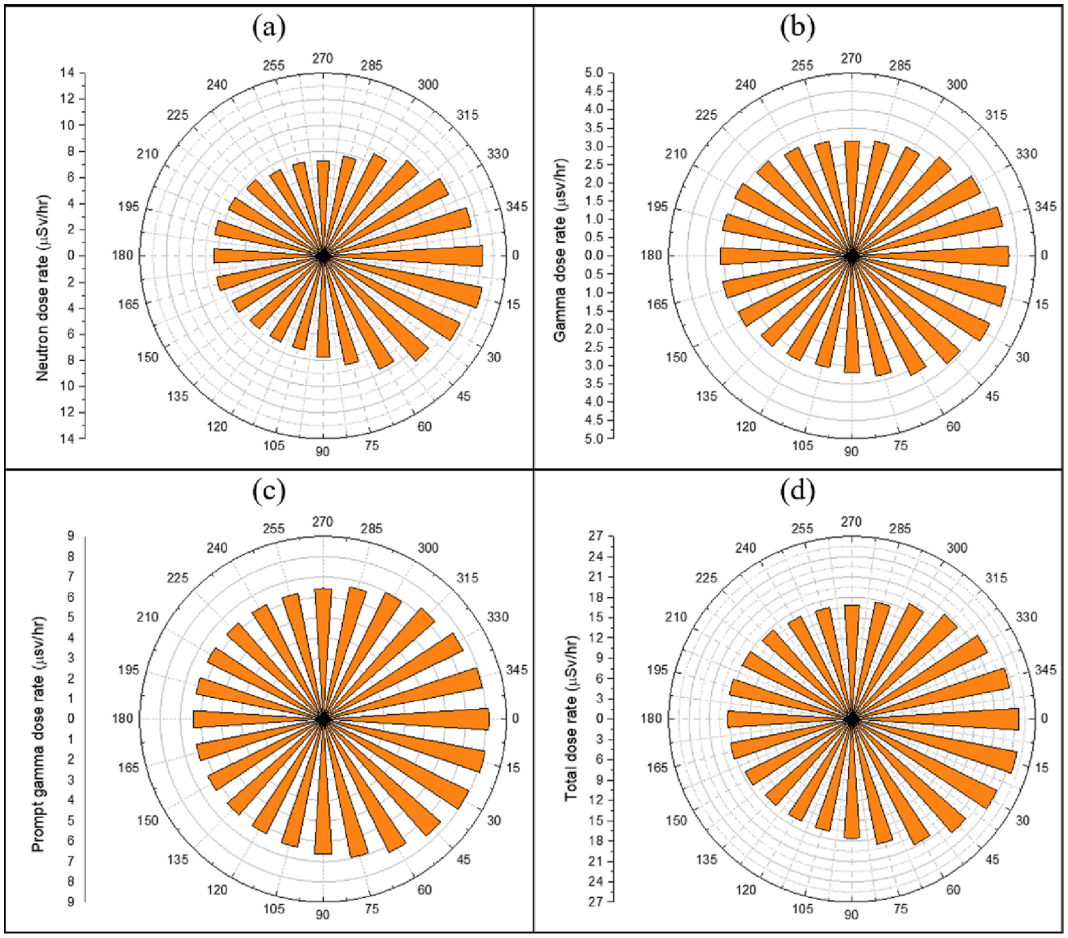

Fig. 2. Radiation dose rate on the outer surface of the irradiator. (a) neutron dose rate, (b) gamma dose rate (4.4 MeV), (c) prompt gamma dose rate, and (d) the total dose rate.

$$G_{Th} = \frac{1}{1 + \left[\frac{N_{Av} K_{Th} m \sigma_{Th}}{r(r+h)A}\right]^{0.964}} \tag{5}$$

$$G_{Epi} = \frac{1}{1 + \left[\frac{N_{Av} k_{Epi} \; m \sigma_{Epi}}{r(r+h)A}\right]^{0.82}} + 0.06 \tag{6}$$

here, N_{Av} is Avogadro's number; r and h are the radii and the height of the sample (gold foil), respectively; A is the atomic number; k_{Th} and k_{Epi} are the thermal and epithermal self-shielding constants, respectively; m is the mass of the foil in grams.

Experimental measurements

Bare gold foils were put in the irradiation sites 1 and 2 for 24 h. In this procedure, some of the gold nuclei would be activated by either thermal or epithermal neutrons. Then, they were taken to the gamma spectroscopy lab, where their 411 keV gamma-ray activities were measured using an HPGe detector with the 767 system shield (front opening split-top lead shield) (Canberra, UK); the HPGe detector is irreplaceable in nuclear radiation characterization and measurements.

The same procedures were conducted on gold foils covered with cadmium of 1 mm in thickness to shield against thermal neutrons. Here, the gold nuclei would only be activated by epithermal neutrons. After 24 h, these foils were transferred to the HPGe detector to measure their 411 keV gamma-ray activities. Depending on the measured activities and their subtraction, the thermal and epithermal fluxes were calculated using Eqs. (3) and (4).

Results and discussion

Radiation protection

A cylindrical irradiator shape was suggested. Two factors were under consideration: 1) as low radiation dose rate possible on the outer surface of the irradiator due to neutron and gamma rays. 2) the irradiator weight must be reasonable. Several MCNP5 simulation trials were conducted to reach the optimal dimensions of the irradiator. Fig. 1a and b show the irradiator's cross-section and top views, respectively. Three components of radiation contribute to radiation hazards: neutrons, gamma-rays (4.44 MeV), and prompt gamma-rays that emerge from neutron interaction with the irradiator materials. It was found that the height (H) is 90 cm, and the diameter (D) is 90 cm. The dose rates due to radiation on the outer surface of the irradiator were calculated using the cylindrical mesh tally. The irradiator in these dimensions could serve as a good shield against radiation. The total dose rate at 1 m from the outer surface was calculated to be 1.39 μSv/hr from neurons (0.48 μSv/hr), gamma rays at 4.4 MeV (0.31 μSv/hr), and prompt gamma rays (60 μSv/hr).

Fig. 2 shows the irradiator's dose rate on the surface due to the three components of radiation mentioned above. Fig. 2a – c show the irradiator's dose rate from the neutrons dose, gamma (4.4 MeV), and prompt gamma, respectively. While Fig. 2d presents the total dose rate, which is 24 μSv/hr at the 0° direction (source 1, large source); it is 15.25 μSv/hr at 180° direction (source 2, small source). At 90° and 270° directions, the dose rate was less than 15 μSv/hr. It can be found that the neutrons contributed is more than 50% at 0° direction relative to source 1, while the contribution due to gamma-rays (4.4 MeV) and prompt gamma-rays

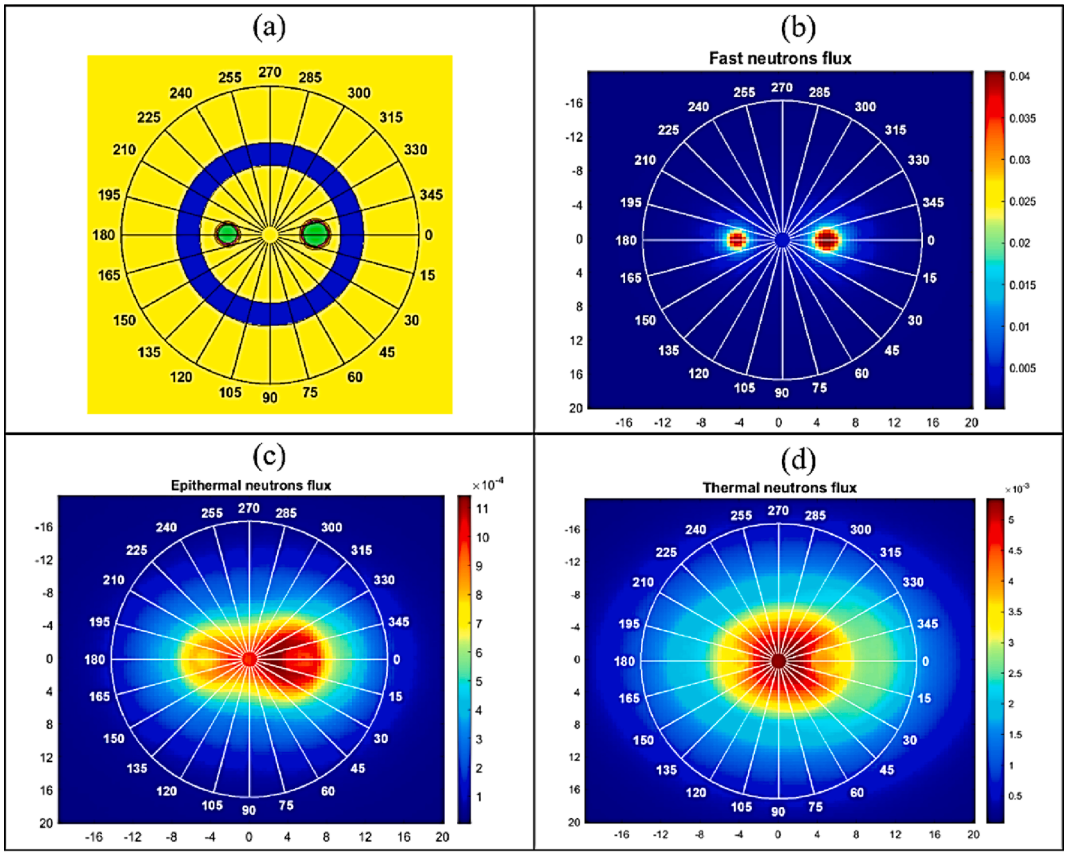

Fig. 3. Neutron fluence (neutron per cm^2 per) inside the irradiator as a function of angle. (a) view of the considered area inside the irradiator 20 cm by 20 cm, (b) fast neutron fluence distribution, (c) epithermal neutron fluence distribution, and (d) thermal neutron fluence distribution.

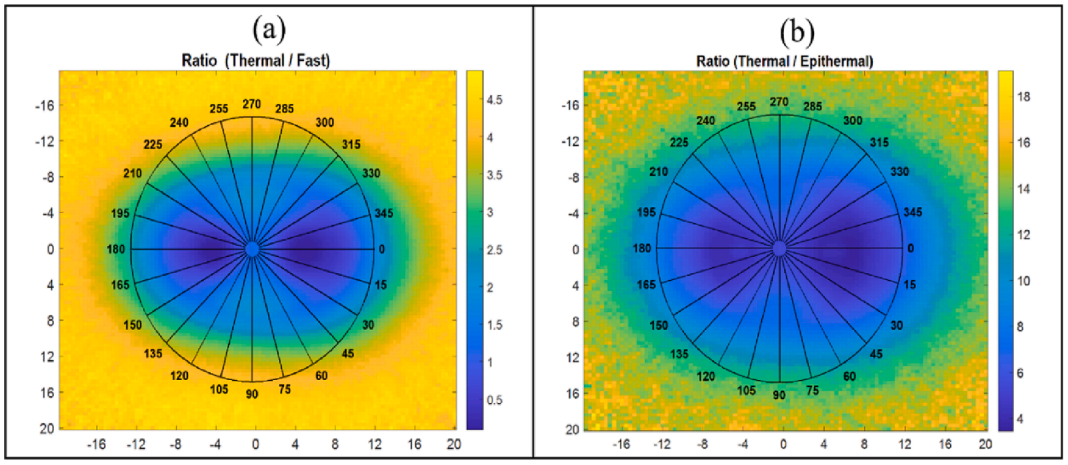

Fig. 4. (a) The ratio of thermal fluence to epithermal fluence and (b) the ratio of thermal fluence to fast fluence.

16% and 33%, respectively.

Neutron fluence mapping

Positioning the irradiation sites inside the irradiator required an image of the neutron fluence distribution. Fig. 3a represents the area under consideration; it was 20 cm by 20 cm at the center of the irradiator. The distribution of the fast neutron fluence is shown in Fig. 3b; at the same time, the epithermal fluence is presented in Fig. 3c, and the thermal fluence is illustrated in Fig. 3d. From these figures, one can recognize that the optimal position for getting the highest neutron fluence of thermal and fast neutrons is the center between the two sources. Accordingly, the first irradiation site has been chosen at the center (site 1).

Fig. 4a shows the thermal-to-fast ratio; thermal fluence is overwhelming the fast one, obviously everywhere outside the lead cylinder. The epithermal fluence is overwhelmed by the thermal fluence everywhere (Fig. 4b). Therefore, irradiation site 2 should be positioned either 90° or 270° right outside the lead cylinder; site 2 was chosen, where the thermal fluence overwhelms the fast fluence. In site 1, which is at the irradiator's center, the thermal fluence percentage was found to be less than 50% of the total fluence.

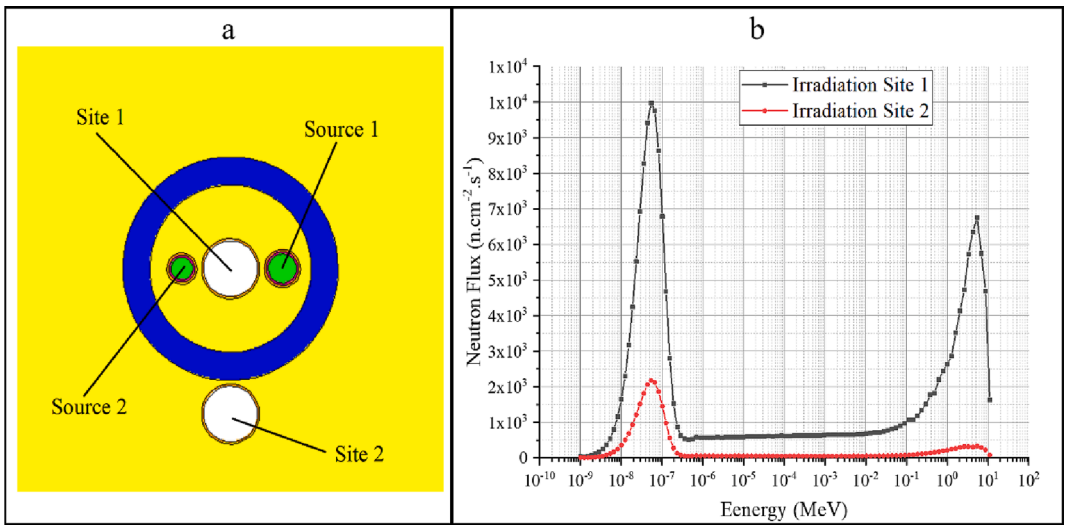

Fig. 5. (a) Positions of irradiation sites 1 and 2 that are relative to neutron sources (b) neutron spectra at site 1 and site 2.

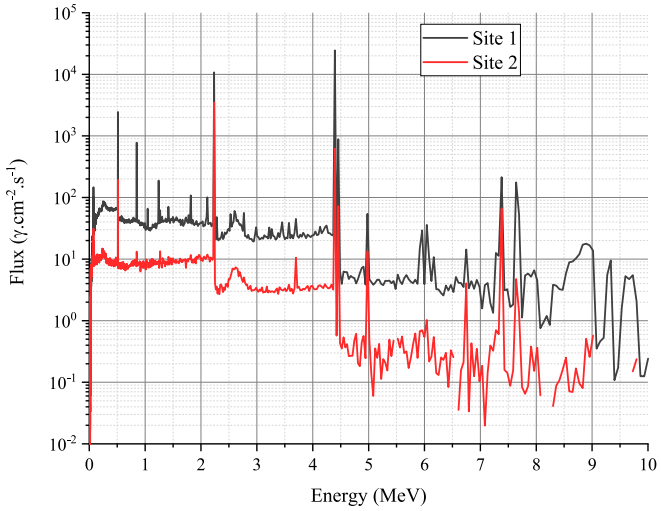

Fig. 6. Gamma-rays spectrum at irradiation sites.

Neutron spectrum and flux at the irradiation sites

After the two irradiation sites were determined, as presented in Fig. 5a, the neutron spectrum and flux were determined. Fig. 5b shows the neutron spectra in sites 1 (black line curve) and 2 (red line curve). Since the site 1 position is near the sources, the neutron flux in site 1 is almost 7 times that in site 2. From Fig. 5b, in sit 1, it can be seen that the thermal flux is 9.24×10^{4}n.cm^{-2}.s^{-1}; this value represents around 49% of the total flux in site 1. At the same time, it is 1.97×10^{4}n.cm^{-2}.s^{-1} in site 2, representing nearly 73% of the total flux in site 2. Besides, in site 1, the fast neutron flux is 6.32×10^{4}n.cm^{-2}.s^{-1}, representing nearly 34%; in the site 2, it is 4.12×10^{3}n.cm^{-2}.s^{-1}, representing around 16%. Also, The epithermal flux is 3.25×10^{4}n.cm^{-2}.s^{-1} (17%) and 3.09×10^{3}n.cm^{-2}.s^{-1} (11%) in sites 1 and 2, respectively.

Gamma-ray spectra at irradiation sites

The gamma-ray spectra in irradiation sites 1 (black line curve) and 2 (red line curve) are presented in Fig. 6. There are three peaks, which are the most intense peaks over the spectrum, namely, 4.44 MeV that comes directly from the two ^{241}Am-^{9}Be sources; 2.2 MeV that emerges due to the reaction ^{1}H(n,γ)^{2}H (prompt gamma); and 0.511 MeV due to positron annihilation. The other peaks emerge due to the inelastic interaction between fast neutrons and iron (Neutron sources capsules were simulated as stainless steel) and the lead nuclei (lead shield).

Table 2
The calculated radiation dose rate in units of mSv/hr for both irradiation sites.

Site	Neutrons	Prompt gamma	Gamma (4.4 MeV)	Total
1	92.81	0.73	2.14	95.68
2	6.62	0.02	0.01	6.65

Radiation exposure at irradiation sites

Table 2 summarizes the delivered dose rate in the irradiation sites; the dose rate in site 1 delivered due to neutrons contributes 92.81 mSv/hr, representing ~97%; gamma-rays (4.44 MeV) deliver 2.14 mSv/hr, representing almost 2%; and prompt gamma rays contribute 0.73 mSv/hr (1%). At the same time, the dose rate due to neutrons in site 2 is 6.65 mSv/hr, which is more than 99%; less than 1% due to both gamma rays (4.44 MeV) (0.01 mSv/hr) and prompt gamma (0.02 mSv/hr).

Experimental estimation of neutron flux in irradiation sites

After the simulations were performed, the irradiator was designed accordingly. Fig. 7 shows photograph images of the designed irradiator from the side and top views (Fig. 7a and b). It can be seen that the entrances of the two sites were taken into consideration during the simulation calculations; these two sites can be used for irradiating the samples.

Using ^{197}Au 411 keV gamma-ray, both thermal and epithermal neutron fluxes in irradiation sites were determined through simulation; the simulation neutron fluxes results, besides the 411 keV activity, are presented in Table 3. Additionally, they were determined experimentally; the experimental results also were listed in the table. The ^{197}Au 411 keV gamma-ray activities were measured using the HPGe detector shown in Fig. 8.

The experimentally estimated thermal neutron flux φ_{Th} in irradiation site 1 is 8.93×10^{4}n.cm^{-2}.s^{-1} and 1.86×10^{4}n.cm^{-2}.s^{-1} in irradiation site 2. The experimentally estimated epithermal neutron flux in irradiation site 1 was determined as 3.44×10^{4}n.cm^{-2}.s^{-1} and 3.37×10^{3}n.cm^{-2}.s^{-1} in irradiation site 2. As shown in Table 3, the differences between the simulation and the experiment results of thermal neutron fluxes in sites 1 and 2 were 3% and 6%, respectively. At the same time, the differences between the simulation and experiment results of epithermal neutron

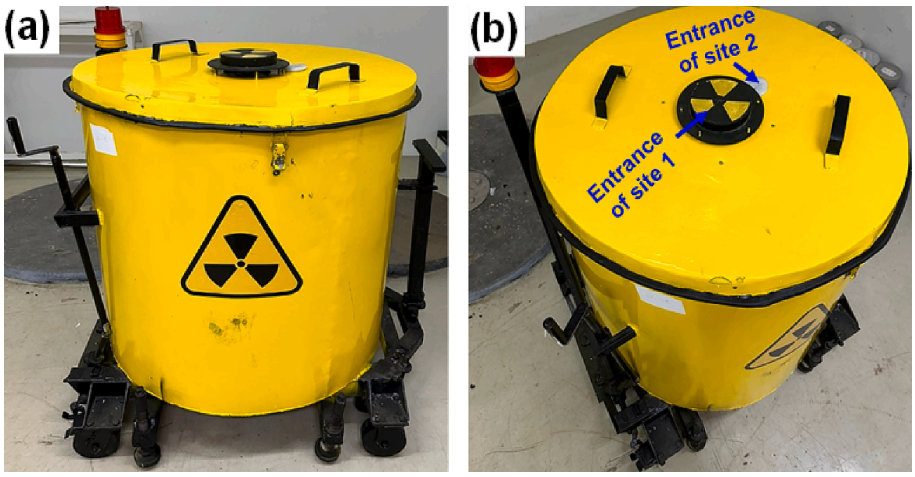

Fig. 7. Photograph images of the designed irradiator. Images (a) and (b) show the side and top views, respectively; the arrows point to the entrances of sites 1 and 2.

Table 3
Simulated and measured gamma-ray 411 keV activity and neutron flux at the irradiation sites 1 and 2.

Parameters	φ_{Th} (n.cm^{-2}.s^{-1})		φ_{Epi} (n.cm^{-2}.s^{-1})		Activity (Bq)			
	Site 1	Site 2	Site 1	Site 2	Site 1		Site 2	
					Bare foil	Foil + Cd	Bare foil	Foil + Cd
Simulated	9.24×10^{4}	1.97×10^{4}	3.25×10^{4}	3.09×10^{3}	798±2%	90±2%	164±2%	10±2%
Measured	8.93×10^{4}	1.86×10^{4}	3.44×10^{4}	3.37×10^{3}	763±28	92±9%	153±12	9±3
Simulated/measured	1.03	1.06	0.94	0.92	1.05	0.98	1.07	1.11

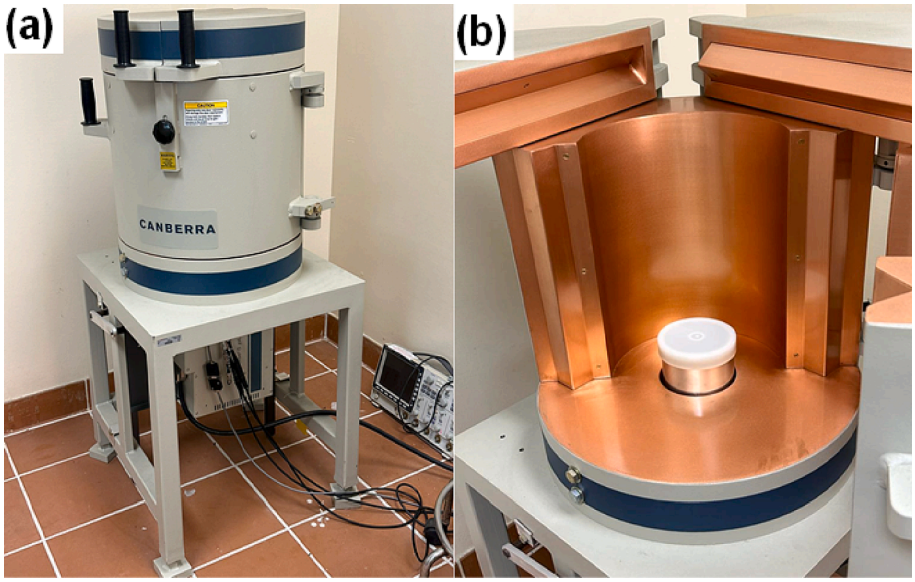

Fig. 8. HPGe detector system. (a) a detector shielding closed (b) open shield.

fluxes in sites 1 and 2 are 6% and 8%, respectively. Generally, simulation and measurement fluxes are in excellent agreement, as found in the ratio of simulation/measured, which is listed in Table 3.

Conclusion

This work presented the stages of the design and the characterization of the two ^{241}Am-^{9}Be neutron sources irradiation facilities in the labs. The MCNP capabilities were utilized to process through all the stages. According to the simulation results, this facility has 1.88×10^{5}n.cm^{-2}.s^{-1} in irradiation site 1, 49% is thermal, and 34% is fast neutrons. In irradiation site 2, the total flux is 2.69×10^{4}n.cm^{-2}.s^{-1}, where 73% thermal neutrons and 16% fast neutrons only. Experimental estimation of the thermal neutron flux was conducted to investigate the accuracy of simulation calculations; the thermal neutron flux in irradiation sites 1 and 2 is 8.93×10^{4}n.cm^{-2}.s^{-1} and 1.86×10^{4}n.cm^{-2}, respectively. The simulation and experimental results have shown excellent agreement in both irradiation sites. The finding of this study is that two ^{241}Am-^{9}Be neutron sources could be merged as one neutron source for applications in the labs.

CRediT authorship contribution statement

Mohammed M. Damoom: Conceptualization, Data curation, Formal analysis, Investigation, Methodology, Funding acquisition, Software, Writing – original draft. **Abdulsalam M. Alhawsawi:** Conceptualization, Project administration, Validation. **Essam Banoqitah:** Conceptualization, Data curation, Formal analysis. **Mohammed Siddig H. Mohammed:** Validation, Writing – review & editing. **Eslam Taha:** Validation, Writing – review & editing. **Yahya Z. Hazzaa:** Investigation, Writing – original draft. **Rayan B. Fawrah:** Investigation, Writing – original draft. **M.M.T. Qutub:** Investigation, Writing – original draft. **Abdu Saeed:** Conceptualization, Methodology, Validation, Writing – review & editing.

Declaration of Competing Interest

The authors declare that they have no known competing financial interests or personal relationships that could have appeared to influence the work reported in this paper.

Data availability

Data will be made available on request.

Acknowledgments

The Deanship of Scientific Research (DSR) at King Abdulaziz University (KAU), Jeddah, Saudi Arabia, has funded this Project under grant no. (G: 687-135-1443). The authors, therefore, acknowledge the DSR technical and financial support.

References

[1] Parry SJ. Activation analysis | Neutron Activation. In: Worsfold P, Townshend A, Poole C, editors. Encyclopedia of Analytical Science (Second Edition). Oxford: Elsevier; 2005. p. 1–10.
[2] Glascock MD. 15.15 - Nuclear Spectroscopy. In: Holland HD, Turekian KK, editors. Treatise on Geochemistry (Second Edition). Oxford: Elsevier; 2014. p. 273–90.
[3] Collins ED, Ottinger CL. Isotopes, Separation and Application. In: Meyers RA, editor. Encyclopedia of Physical Science and Technology (Third Edition). New York: Academic Press; 2003. p. 109–26.
[4] Jiang H, Winder DE, Barbier C, Riemer BW. Implementing bubbly mercury material model (R-P model) in the pulse simulation to predict strain on the Spallation Neutron Source target vessel with gas injection. Results Phys 2023;49:106511.
[5] Radaideh MI, Lin L, Jiang H, Cousineau S. Bayesian inverse uncertainty quantification of the physical model parameters for the spallation neutron source first target station. Results Phys 2022;36:105414.
[6] Fu X, Wei B, Kang J, Wang W, Tang G, Li Q, et al. Fast neutron irradiation effects on Si- and GaN-based avalanche photodiodes. Results Phys 2022;38:105574.
[7] Fu X, Kang J, Tang G, Chen F, Li Q, Li M, et al. Fast neutron irradiation effects on AlGaN deep ultraviolet light emitting diodes. Results Phys 2021;27:104532.
[8] Harrison RJ. Neutron Diffraction of Magnetic Materials. Rev Mineral Geochem 2006;63(1):113–43.
[9] Winkler B. Applications of Neutron Radiography and Neutron Tomography. Rev Mineral Geochem 2006;63(1):459–71.
[10] Winkler B, Knorr K, Kahle A, Vontobel P, Lehmann E, Hennion B, et al. Neutron imaging and neutron tomography as non-destructive tools to study bulk-rock samples. J European Journal of Mineralogy 2002;14(2):349–54.
[11] Baranov V, Davydov YI, Erasmus R, Kureba CO, Lekalakala N, Masuku T, et al. Effects of neutron radiation on the optical and structural properties of blue and green emitting plastic scintillators. Nucl Instrum Methods Phys Res, Sect B 2018;436:236–43.
[12] Vali IP, Shetty PK, Mahesha MG, Rao MN, Kesari S. Thermal neutron irradiation effects on structural and electrical properties of n-type 4H-SiC. J Mater Sci-Mater Electron 2020;31(11):8496–501.
[13] Santa SA, Suwoto. Suwoto, Neutron Radiation Damage Estimation in the Core Structure Base Metal of RSG GAS. J Phys Conf Ser 2018;962:012050.
[14] Stopher MA. The effects of neutron radiation on nickel-based alloys. Mater Sci Technol 2017;33(5):518–36.
[15] Saeed A, Murshed MN, Al-Shahari EA. Effect of low-dose fast neutrons on the protein components of peripheral blood mononuclear cells of whole-body irradiated Wistar rats. Environ Sci Pollut Res 2020;27(32):40443–55.
[16] Nafee SS, Saeed A, Shaheen SA, El Assouli SM, Assouli MZE, Raouf GA. Effect of very low dose fast neutrons on the DNA of rats' peripheral blood mononuclear cells and leukocytes. Health Phys 2016;110(1):50–8.
[17] Saeed A, Raouf GA, Nafee SS, Shaheen SA, Al-Hadeethi Y, Perc M. Effects of very low dose fast neutrons on cell membrane and secondary protein structure in rat erythrocytes. PLoS One 2015;10(10):e0139854.
[18] Saeed A, Abolaban F. Risk estimation of the low-dose fast neutrons on the molecular structure of the lipids of peripheral blood mononuclear cells. Biochem Biophys Res Commun 2020;533(4):1048–53.
[19] Saeed A, Abolaban F. Spectroscopic study of the effect of low dose fast neutrons on the hemoglobin structure. Spectrochim Acta, Part A 2021;261:120082.
[20] Boulet-Roblin L, Sheptyakov D, Borel P, Tessier C, Novák P, Villevieille C. Crystal structure evolution via operando neutron diffraction during long-term cycling of a customized 5 V full Li-ion cylindrical cell LiNi0.5Mn1.5O4vs. graphite. J Mater Chem A 2017;5(48):25574–82.
[21] Kafala SI, MacMahon TD. Comparison of neutron activation analysis methods. J Radioanal Nucl Chem 2007;271(2):507–16.
[22] Rinaldi R, Liang L, Schober H. Neutron Applications in Earth, Energy, and Environmental Sciences. In: Liang L, Rinaldi R, Schober H, editors. Neutron Applications in Earth. Springer, US, Boston, MA: Energy and Environmental Sciences; 2009. p. 1–14.
[23] Asamoah M, Nyarko BJB, Fletcher JJ, Sogbadji RBM, Yamoah S, Agbemava SE, et al. Neutron flux distribution in the irradiation channels of Am–Be neutron source irradiation facility. Ann Nucl Energy 2011;38(6):1219–24.
[24] Mowlavi AA, Koohi-Fayegh R. Determination of 4.438MeV γ-ray to neutron emission ratio from a 241Am–9Be neutron source. Appl Radiat Isot 2004;60(6):959–62.
[25] Shtejer-Diaz K, Zamboni CB, Zahn GS, Zevallos-Chávez JY. Determination of neutron flux distribution in an Am–Be irradiator using the MCNP. Appl Radiat Isot 2003;59(4):263–6.
[26] Hu Q, Jia W, Hei D, Li J, Cheng C, Zhao D. Design of a controllable Am–Be neutron source: A Geant4 simulation. Appl Radiat Isot 2021;174:109775.
[27] Mensimah E, Abrefah RG, Nyarko BJB, Fletcher JJ, Asamoah M. Neutron flux determination in irradiation sites of an Am–Be neutron source at NNRI. Ann Nucl Energy 2011;38(10):2303–8.
[28] Saeed A, Nafee SS, Shaheen SA, Raouf GA, Al-Hadeethi Y, Kamal SM, et al. Calculating the ambient dose equivalent of fast neutrons using elemental composition of human body. Appl Math Comput 2016;274:604–10.
[29] Croft S. The use of neutron intensity calibrated 9Be(α, n) sources as 4438 keV gamma-ray reference standards. Nucl Instrum Methods Phys Res, Sect A 1989;281(1):103–16.
[30] EF Shores, Contact dose equivalent rates from common neutron sources, Los Alamos National Lab.(LANL), Los Alamos, NM (United States), Washington. 2000.
[31] El-Sersy AR, Eman SA, Khaled NE. Fast neutron spectroscopy using CR-39 track detectors. Nucl Instrum Methods Phys Res, Sect B 2004;226(3):345–50.
[32] Zhang X, Yang M, Zhang X, Wu H, Guo S, Wang Y. Enhancing the neutron shielding ability of polyethylene composites with an alternating multi-layered structure. Compos Sci Technol 2017;150:16–23.
[33] Vega-Carrillo HR, Manzanares-Acuña E, Becerra-Ferreiro AM, Carrillo-Nuñez A. Neutron and gamma-ray spectra of 239PuBe and 241AmBe. Appl Radiat Isot 2002;57(2):167–70.
[34] Hancock RGV. Low flux multielement instrumental neutron activation analysis in archaeometry. Anal Chem 1976;48(11):1443–5.
[35] Nyarko BJB, Akaho EHK, Serfor-Armah Y. Application of NAA standardization methods using a low power research reactor. J Radioanal Nucl Chem 2003;257(2):361–6.
[36] Papastefanou C. Measurement of neutron flux and albedo of water for thermal neutrons with foils of indium in a subcritical nuclear reactor. J Radioanal Nucl Chem 2004;261(3):671–8.
[37] Ingelbrecht C, Peetermans F, De Corte F, De Wispelaere A, Vandecasteele C, Courtijn E, et al. D'Hondt, Aluminium-gold reference material for the k0-standardisation of neutron activation analysis. Nucl Instrum Methods Phys Res, Sect A 1991;303(1):119–22.
[38] Poularikas A, Cunningham J, McMillan W, McMillan J, Fink RW. New isomers of scandium-50 and indium-120; γ-rays in lutecium-178 decay. J lnorg Nucl Chem 1960;13(3):196–9.
[39] IAEA. Prompt gamma-ray neutron activation analysis. International Atomic Energy Agency. 2014.
[40] Haddad K, Anjak O, Yousef B. Neutron and high energy photon fluence estimation in CLINAC using gold activation foils. Reports of Practical Oncology & Radiotherapy 2019;24(1):41–6.
[41] Chilian C, St-Pierre J, Kennedy G. Dependence of thermal and epithermal neutron self-shielding on sample size and irradiation site. Nucl Instrum Methods Phys Res, Sect A 2006;564(2):629–35.